High entropy spinel oxides for water oxidation: surface entropy evolution and activity promotion

Jiarui Wang[1,5], Shengnan Sun[2,5], Shibo Xi[3], Yuanmiao Sun[4], Samuel Jun Hoong Ong[1], Zhi Wei Seh[2], Zhichuan J. Xu[1]*

[1] School of Materials Science and Engineering, Nanyang Technological University, 50 Nanyang Avenue, Singapore 639798, Republic of Singapore.

[2] Institute of Materials Research and Engineering (IMRE), Agency for Science, Technology and Research (A*STAR), 2 Fusionopolis Way, Innovis #08-03, Singapore 138634, Republic of Singapore.

[3] Institute of Sustainability for Chemicals, Energy and Environment (ISCE²), Agency for Science, Technology and Research (A*STAR), 1 Pesek Road, Jurong Island, Singapore 627833, Republic of Singapore

[4] Faculty of Materials Science and Energy Engineering/Institute of Technology for Carbon Neutrality, Shenzhen Institute of Advanced Technology, Chinese Academy of Sciences, Shenzhen 518055, China.

[5] These authors contributed equally: Jiarui Wang, Shengnan Sun.

* Corresponding author: Zhichuan J. Xu (xuzc@ntu.edu.sg)

Abstract

In recent years, the concept of entropy stabilization has led to increased research in "high entropy materials". These compounds incorporate multiple metals into a single crystalline phase, resulting in interactions between them that offer novel and unexpected properties. Here, we report on the surface evolution and entropy changes of the high entropy spinel oxide (HEO) $Zn(CrMnFeCoNi)_2O_4$ upon its use as an electrocatalyst for the oxygen evolution reaction (OER). It was found that electrochemical cycling of this material results in surface reconstruction accompanied by induced leaching of surface Zn from tetrahedral sites. The formation of a

completely new metal (oxy)hydroxide $Zn_2Cr_{1.5}Mn_2Fe_1Co_2Ni_{1.5}O_xH_y$ is observed at the surface, leading to an increase in surface entropy over the pristine spinel HEOs. The newly formed surface exhibits improved OER catalytic performance, through the adsorbate evolution mechanism (AEM). Removing any one of the cations from this HEO results in a significant drop in OER performance. This shows that the electrochemical behavior of the high entropy oxides depends on each of the metal ions present on the catalyst's surface, thus providing the opportunity to tailor its electrochemical properties by simply changing the elemental composition.

Introduction

Hydrogen plays a pivotal role as a primary energy carrier in the decarbonization of energy infrastructure Electrochemical water splitting using sustainable energy is a promising technology for green hydrogen generation.[1] The oxygen evolution reaction (OER) is the anode reaction in electrochemical water splitting, which requires a high overpotential due to its being a four-step electron transfer process with multiple reaction intermediates.[2-5] Depending on the type of electrolyzers, the anode catalysts can be different in materials. For example, noble metals are used in membrane electrode assembly electrolzyers using a proton exchange membrane, which provides a strong acidic condition and only novel metals can survive. As a result, the cost is a major concern.[6-8] In alkaline water electrolysis, the working condition of the anode is more friendly to most transition metals and their oxides or oxyhydroxides can be stable under such conditions.[9-11] Recent studies have revealed that most metal oxides that act as OER catalysts undergo a surface phase change, or surface reconstruction, to oxyhydroxides, which are more stable under alkaline conditions.[3, 11-13] Such a change is usually accompanied with a change in OER performance.[14] Thus, instead of the bulk phase of most catalysts, the oxyhydroxides generated on the surface under operating conditions are often believed to be the real catalysts for the OER.

To promote the activity by surface reconstruction, some effort has been made in activate the lattice oxygen in order to make the oxides less stable. For example, lattice oxygen can be activated by substituting Co by Ni in $ZnCo_2O_4$, and the metastable spinel oxide can be made at an optimal substitution level.[15] The lattice oxygen oxidation mechanism (LOM) of OER can be activated and cycling the catalyst results in a significant improvement in OER performance. A recent study has also found that the covalency of bonds in the material can be used as a design principle for spinel

pre-catalyst.[3] In addition, the cation leaching is also a commonly observed phenomenon that triggers the surface reconstruction.[15]

Most recently, several studies have reported that high entropy materials (HEMs) exhibit great potential in electrocatalysis.[16-18] For example, Jia *et al.* incorporated the concept of high entropy alloy into a high-entropy metallic glass for hydrogen production, which shows better activity than most catalysts.[19] A greater grouping of HEMs is the category of oxides known as high entropy oxides (HEO), which are mixed-metal oxides with five or more different cations in equal atomic ratio.[18, 20-22] Since Rost *et al*. synthesized the first HEO in 2015, HEOs attracted great attention.[22] As a new class of oxide system, HEOs are formulated by the concept of entropy stabilization, which allows for a HEO to thermodynamically accommodate multiple metal species in various crystal phases.[21] However, the advantages of using HEOs as catalysts have not been fully revealed. The enormous number of possible elemental combinations has the potential to yield unexpected properties and performance. The opportunity to tailor the electron band of a HEO by combining various elements and their structures also provides opportunities to manipulate the electrocatalytic activity of a HEO.[23, 24] Although HEOs have been reported giving high performance in electrocatalysts,[16-18] their surface stability has not yet been studied. As introduced above, the OER is tough reaction to the structures of electrocatalysts. Their instability and tendency to undergo surface reconstruction under OER conditions necessitates the study of these behaviours in the case of HEOs to fully understand their application in OER electrocatalysis.

Here, we report a highly active spinel type HEO, $Zn(CrMnFeCoNi\text{-}X)_2O_4$ for OER. The incorporation of Zn aims to fix the spinel to a normal structure and therefore allow for information on the catalytically critical octahedra to be gained. During OER performance, the OER pathway undergoes a transformation from concerted proton-electron transfer to non-concerted proton-electron transfer. A step-by-step investigation of HEO by surface-sensitive tools is also carried out. A thin layer of metal (oxy)hydroxide (MO_xH_y) was found to be formed after a few hundred cycles of CV. It is also found that the further loss of surface cations increases the surface entropy of the HEO compared to its original spinel state. This increased surface entropy is also found to be associated with improved OER performance. Finally, the construction of similar HEOs excluding a single element leads to decreased electrochemical performance, further indicating the positive effect of high entropy on OER catalysis.

Methods

Synthesis of HEO/MEO Particles

The spinel HEO/MEOs were synthesized by a low-temperature sol-gel method. All chemicals were obtained from Sigma-Aldrich and used as-is. First, a mixture of 30 mmol of acetate salts (composed of stoichiometric amounts of $Zn(CH_3COO)_2 \cdot 2H_2O$, $Mn(CH_3COO)_2 \cdot 4H_2O$, $Cr_3(CH_3COO)_7(OH)_2$, $Fe(NO_3)_3 \cdot 9H_2O$, $Co(CH_3COO)_2 \cdot 4H_2O$ and $Ni(CH_3COO)_2 \cdot 4H_2O$) and 90 mmol of citric acid was dissolved in 200 mL of deionized water (DI water) to form an aqueous solution. After adding 20 mL of nitrite acid, the solution was heated and stirred at 90 °C until a homogeneous gel formed. Then the gel was heated at 170 °C for 12 h to form the resin, followed by annealing at 600 °C in the air for 6 h. The as-prepared HEO/MEOs were used as active oxygen oxidation material without any further heat treatment step.

Electrode Preparation

Oxide electrodes were prepared by drop-casting the ink of catalysts onto glassy carbon electrodes (GCEs) with a geometric surface area of 0.196 cm^2. HEO/MEOs and acetylene black (AB) were dispersed in ethanol and Nafion perfluorinated resin solution (5 wt % in water) to form a 1.8 mg_{Oxide}/mL mixture. The mass ratio of AB to oxides was maintained at 7:3, and the volume ratio of ethanol to Nafion was kept at 1:0.02. Before drop-casting, the GCE was polished with alumina slurry for 30 minutes, cleaned by repeated ultrasonication in ethanol and DI water, and dried under ambient conditions. The mixture was ultrasonicated for 30 min to achieve a homogeneous dispersion of oxides and AB. Then, the ink was drop-casted and dried at room temperature to evaporate ethanol. A total of 10 μL of ink of HEO/MEOs was dropped onto GCE, yielding an oxide mass loading of 91.84 $\mu g/cm^2_{disk}$.

Electrochemical Measurement

A three-electrode cell configuration consisted of a GC electrode, a platinum sheet, and a Hg/HgO (1.0 M KOH) reference electrode (0.098 V vs. RHE). All cyclic voltammetry (CV) measurements were conducted from 1.03 to 1.63 V (vs. RHE) at a scan rate of 10 mV s^{-1} in 1.0 M KOH electrolyte. All potentials were referenced to the RHE scale and corrected for Ohmic resistance. The resistance

was determined by electrochemical impedance spectra (EIS) measurements. All EIS were recorded at 1.53 V (vs. RHE) with frequencies ranging from 10^5 to 10^{-1} Hz and an AC voltage amplitude of 10 mV.

Material Characterization

The High-resolution transmission electron microscopy (HRTEM) study was carried out on a JEOL 2100 transmission electron microscope at 200 kV and energy-dispersive X-ray (EDX) spectroscopy analysis. The X-ray photoelectron spectroscopy (XPS) was performed by PHI 5000 VersaProbe, and the binding energies were corrected for specimen charging effects using the C 1s level at 284.6 eV as the reference. The X-ray diffraction pattern (XRD) was collected on a PANalytical X'pert Pro with Cu Kα radiation (λ = 1.5418 Å). The FESEM images were recorded on a JEOL FESEM 7600F at 15 kV. An ASAP Tristar II 3020 was used to measure the Brunauer–Emmett–Teller (BET) specific surface area and the average particle size of samples.

Results and discussion

HEO characterization

Figure 1a shows the X-ray diffraction (XRD) pattern of the as-synthesized $ZnCr_{0.4}Mn_{0.4}Fe_{0.4}Co_{0.4}Ni_{0.4}O_4$. The catalyst exhibits a cubic-spinel structure with Fd-3m space group matched to the database entry PDF No. 00-022-1107. The TEM image in Figure S1 shows the particle morphologies and phases of the HEO are in the nano to micrometre range. From the high-resolution TEM (HRTEM) image in Figure 1b, a lattice spacing of 0.256 nm can be found, which matches the crystal facet of (111) and further supports the cubic spinel structure of the as-synthesized HEO. The four diffraction rings in the selected area electron diffraction (SAED) pattern (inset of Figure 1b) are perfectly indexed to the same positions as those in XRD patten.

The site occupations of metal ions were investigated by extended X-ray absorption fine structure (EXAFS) (Figure 1c). The first Fourier transform peak at around 1.5 Å shows the distance between metals and oxygen. The second Fourier transform peak shows the distance between the absorbing

metal ion (Zn, Cr, Mn, Fe, Co, and Ni) and their neighboring cations in either octahedral or tetrahedral sites. The cations have a 2.5 Å metal-metal distance from their neighboring metal ions, suggesting that Cr, Mn, Fe, Co, and Ni reside in the octahedral sites of TM-HEO.[25-28] The distance between Zn ions and their adjacent metal ions, which occupy octahedral sites, is around 3.0 Å. Besides, no peak appears at 2.5 Å. These results indicate that Zn ions in the as-synthesized HEO catalysts accommodate the center of tetrahedrons .[25-28] The spatial distribution of metal ions was also investigated by transmission electron microscopy (TEM) and Energy-dispersive X-ray spectroscopy (EDX). As shown in Figure S1, the elements in the as-synthesized HEO are homogeneously distributed, as no segregation or clustering is observed.

OER performance of HEOs

Activities normalized by the BET surface area are presented in Figure 1d and 1e. The activities are normalized by BET surface areas, which are presented in Figure S2 and Table S1. As can be seen, a remarkable activity increase in OER performance is observed during the first 1000 cycles. After that, the increase slows down until a decrease in current density appears after the 1500th cycle. The electrochemical active surface area (ECSA) of Act-HEO (active HEO) after 1000 CV cycles is higher than that of Pri-HEO (pristine HEO), indicating an increase in the number of active sites after electrochemical cycling (Figure S3). The current density normalized by ECSA of Act-HEO is still higher than that of Pri-HEO, indicating that not only the number of active sites but also the intrinsic activity per site increases during the OER process.[29, 30] Moreover, a reduction in Tafel slope from 124 mV dec^{-1} (Pri-HEO) to 49 mV dec^{-1} (Act-HEO after 2000 CV cycles) is observed, which indicates that the HEO catalyst is also activated towards higher kinetics (Figure 1e).[31] The difference in Tafel slopes suggests a change in the rate-limiting step during OER. Traditionally, the whole OER process can be separated into a four-step reaction, in which each step involves oxygen species adsorption and charge transfer[32, 33]:

$$M–OH + OH^- \rightarrow M–O + H2O + e^- \quad (1)$$

$$M–O + OH- \rightarrow M–OOH + e^- \quad (2)$$

$$M–OOH + OH \rightarrow M–OO + H_2O + e^- \quad (3)$$

$$M–OO + OH^- \rightarrow M–OH + O_2 + e^- \quad (4)$$

In addition, the relationship between current density and potential can be described by the following equation[32, 33]:

$$\eta = 2.303RT/(\alpha F) \times \log i – 2.303RT/(\alpha F) \times \log i_0$$

In above equation, the Tafel slope can be derived as 2.303RT/(0.5 + n)F, in which n is the number of electron-transfer steps before the rate-determining step (RDS) and α is assumed to be 0.5. For different RDS, the catalysts give different Tafel slope values. The Tafel slope of 124 mV dec^{-1} for Pri-HEO indicates that the first electron transfer of the adsorbed OH^- (step 1) is the RDS because there is no electron transfer before the RDS. Then, after around 200 CV cycles, the Tafel value rapidly decreases to 50 mV dec^{-1}, showing that the second step becomes the RDS, where the number of electron-transfers n increases to 1.

In addition to the RDS, the reaction mechanism was examined to give a more accurate determination of the surface evolution of Pri-HEO and Act-HEO. To do this, the OER performances of each material were analyzed using KOH electrolyte with different pH values. The Act-HEO was pretreated in 1 M KOH for 1000 CV cycles. The resulting background and iR-corrected OER curves are shown in Figure 1f and 1g. It is apparent that the catalytic activity of Pri-HEO exhibits strong pH dependence, while the Act-HEO shows no change in OER performance in electrolyte with different pH.[34] Previous research has shown that pH dependence indicates the existence of nonconcerted proton-electron transfer in catalytic reactions.[34, 35] To better illustrate this, alternative concerted proton-electron transfer pathways are displayed in Figure 1h. Specifically, the conventional concerted proton-electron transfer occurs along the diagonal and the two alternative concerted pathways are shown along the edges of the square scheme. According to recent findings, one of the potential pathways of non-concerted proton-electron transfer during OER could involve the redox of lattice oxygen.[36, 37] In addition, under the lattice-oxygen-mediated (LOM) mechanism, the formation of surface V_O (oxygen vacancies) often results from the leaching of surface cations. As the leaching of cations acts as one of the ways to compensate the oxidation process when the filling rate of OH^- (aq) to the surface V_O is not fast enough, surface amorphization is commonly detected over electrochemical cycling for

non-concerned proton-electron transfer.[35-37] The difference in pH dependency highlights a fundamental mechanistic shift from the surface metal ions to conventional OER mechanism over cycling. In addition, the change in OER mechanism also shows the change in metal-oxygen covalencies for Pri-HEO and Act-HEO, which will be further examined by surface sensitive tools.

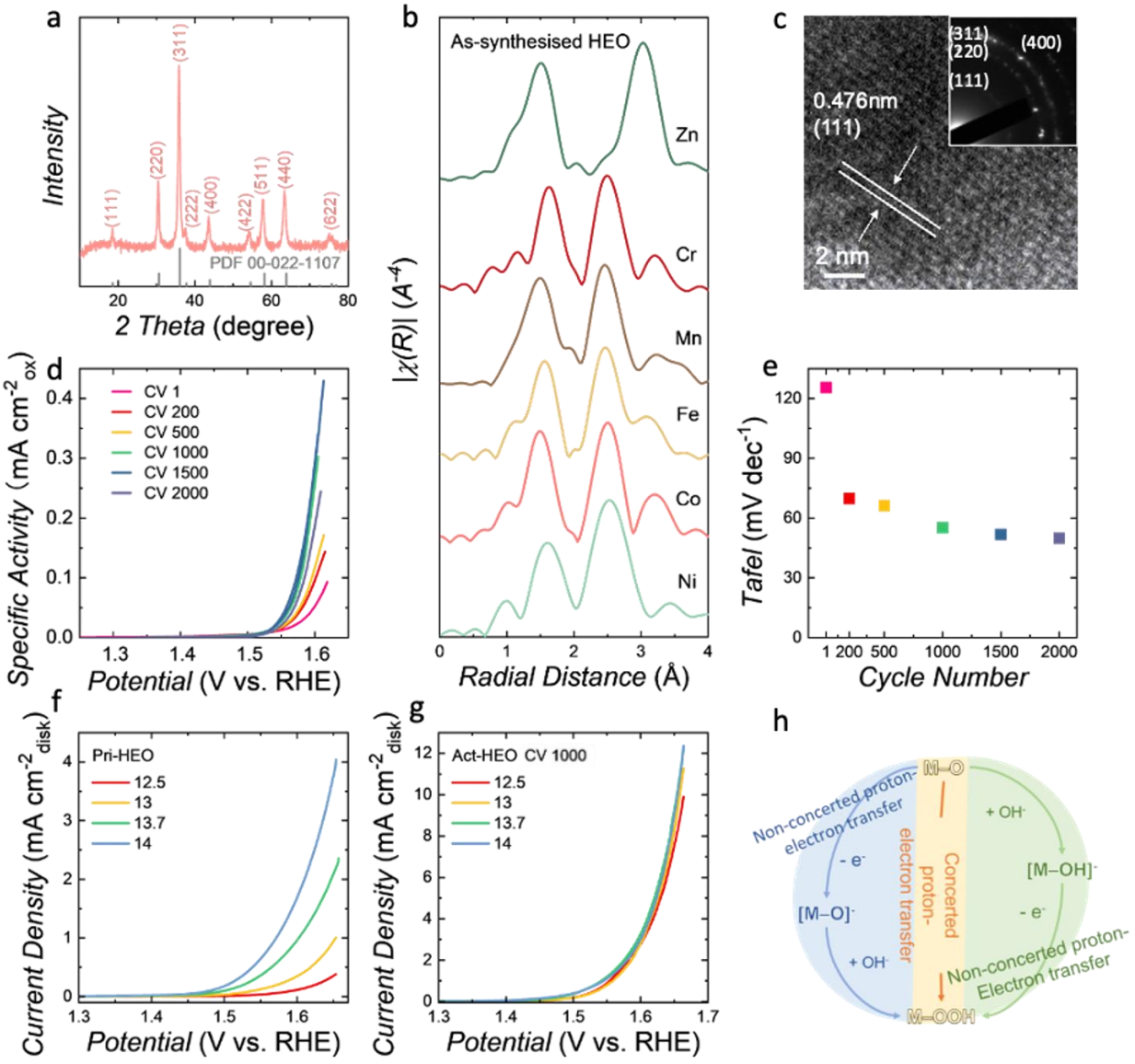

Figure 1: Crystal structure of as-synthesized HEO material $Zn(CrMnFeCoNi)_2O_4$. a) Powder XRD patterns of the as-synthesized HEO catalyst. b) High-resolution TEM (HRTEM) image of as-synthesized HEO. Inset shows the selected area electron diffraction (SAED) pattern of as-synthesized HEO. c) Fourier transform of the EXAFS (FT-EXAFS) for Zn, Cr, Mn, Fe, Co and Ni K-edge of as-synthesized HEO. The second peak at ca. 3.0 Å (i.e. TM_{Td}-TM_{Td} or TM_{Td}-TM_{Oh}) are interatomic metal–metal distances from the absorbing metal ion Cr, Mn, Fe, Co and Ni to

the second nearest-neighbor metal ions at the tetrahedral site. The second peak at ca. 2.5 Å (i.e. TM_{Oh}-TM_{Td} or TM_{Oh}-TM_{Oh}) are interatomic metal–metal distances from the absorbing metal ions to the second nearest-neighbor metal ions at the octahedral site. d) Cyclic voltammetry (CV) curves of HEO at the 1st, 200th, 500th, 1000th, 1500th and 2000th cycles. The characterization was performed at the potential range from 1.23 V to 1.65 V vs. RHE (reversible hydrogen electrode). e) Tafel value of HEO at the 1st, 200th, 500th, 1000th, 1500th and 2000th cycles. f) - g) OER performance of Pri-HEO and Act-HEO in electrolyte with different pH values. h) Diagram of OER reaction pathways.

Surface analysis of active HEO after OER

To further investigate the surface evolution during OER, some bulk and surface characterization techniques were conducted. In Figure 2a, the XRD pattern of Act-HEO after 1000 CV cycles still matches the cubic-spinel structure with Fd-3m space group, indicating that the core structure of the HEO remains stable after CV cycling. However, the HRTEM reveals the formation of an apparently amorphous surface layer without long-range order (Figure 2b and Figure S6), which suggests the presence of metal (oxy)hydroxides on the surface of HEO during the OER process. The thickness of the amorphous layer shown in the HRTEM also remains unchanged after 500 CV cycles (Figure S6). The coordination environment of elements in HEO was further investigated by EXAFS spectra (Figure 2f). The distance between Zn ions and their neighboring metal ions is around 3 Å and no peak can be observed around 2.5 Å. In addition, the distances between other elements are all below 2.5 Å, suggesting that Cr, Mn, Fe, Co, and Ni are in octahedral sites while bulk Zn remains in tetrahedral sites. In short, there is no difference in bulk site occupation between Act-HEO and Pri-HEO. X-ray absorption near edge structure (XANES) measurements with transmission mode were also conducted before and after CV cycling (Figure 2c-e, 2g, and 2h) to examine the oxidation states and core structure of Pri-HEO and Act-HEO. No difference in XANES results can be observed, which indicates that the material's bulk structure remains unchanged after 1000 CV cycles. In addition, the position of the transition metal element K-edge in HEO remains in the same energy domain after activation for 1000 CV cycles at μ=0.5, indicating no change in the average oxidation state of these elements. Therefore, it can be deduced that the core HEO structure remains apparently unchanged after long-term OER reactions. This overall

stability can be attributed to configurational entropy stabilization of the lattice, which preserves the original spinel structure while serving as a permanent host matrix for the conversion cycles.

Several surface characterization tools were also used to analyze Pri-HEO and Act-HEO at different stages. X-ray photoelectron spectroscopy (XPS) was conducted to examine the surface evolution of HEOs with a depth of 2-5 nm.[38] With XPS mapping technology, the surface species' valence state and compositions at different stages can be obtained. Figure 2i-k show the O 1s, Co $2p_{3/2}$ and Ni $2p_{3/2}$ XPS spectra of the Pri-HEO and Act-HEO at 1000th CV cycling. The $2p^{3/2}$ orbitals for surface elements (O, Zn, Cr, Mn, Fe, Co, and Ni) of Pri-HEO and Act-HEO at CV 200th, 500th, 1000th, 1500th and 2000th cycles are shown in Figure S4. Fittings of the experimental spectra obtained for HEO are shown in colored lines. The resulting O 1s spectra can be deconvoluted into two different contributions, with the signals at 529 eV and 532 eV reflecting the presence of lattice oxygen and hydroxide ions, respectively.[39-42] Over 75 % of the surface oxygen species in the Pri-HEO after 200 CV cycles are composed of lattice oxygen. On the other hand, only around 20% of surface lattice oxygen is observed in the case of Act-HEO, which indicates a low probability of lattice oxygen participation, consistent with concerted proton-electron transfer during OER. In addition, compared with Pri-HEO, a slight shift is observed towards the higher binding energy side of surface Cr, Mn, Fe, Ni, and the lower binding energy side of surface Co of Act-HEO, indicating the increased valence state and metal-oxygen covalency of surface cations.

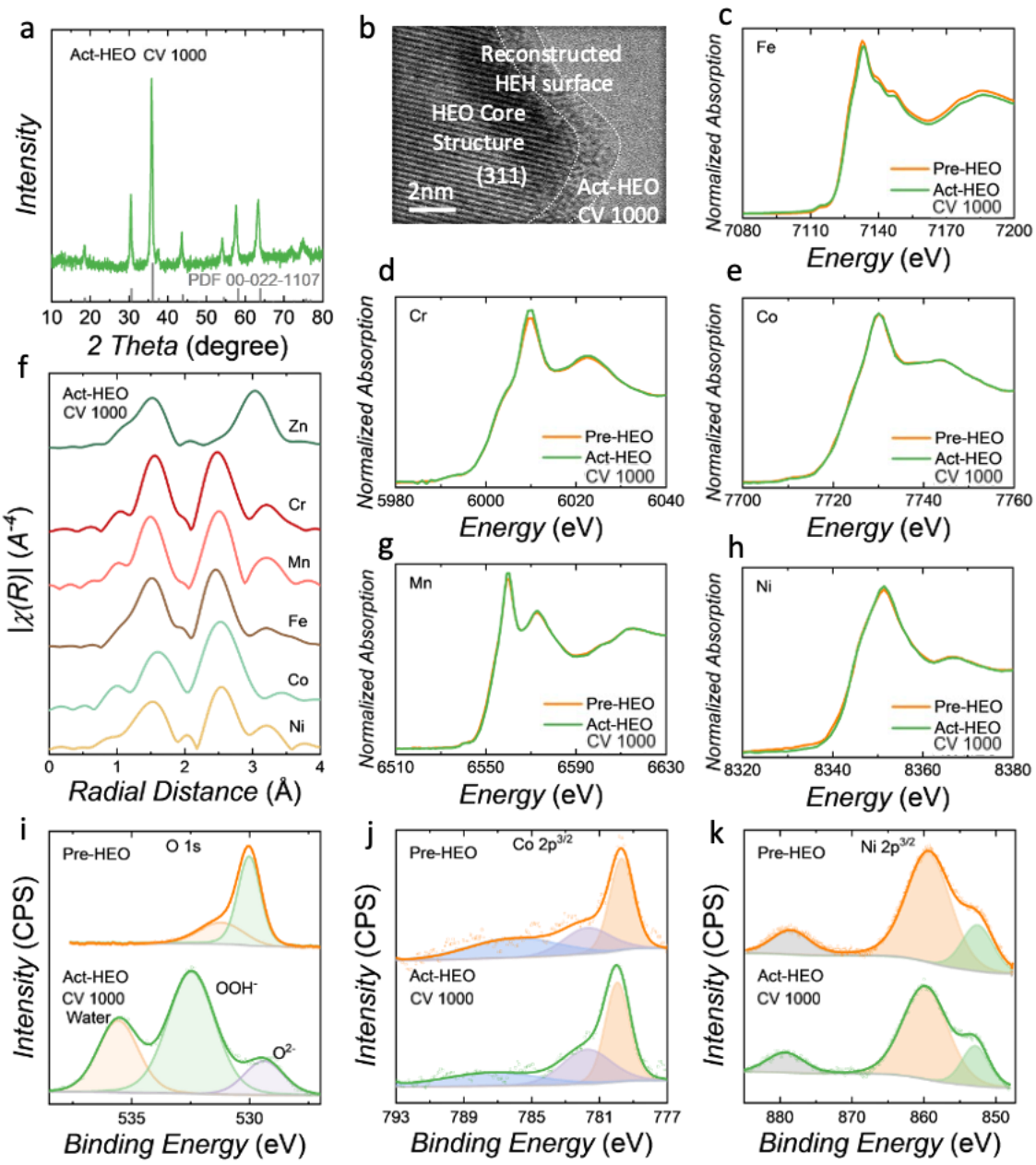

Figure 2: Characterizations of HEO after CV cycling. a) XRD pattern of Act-HEO at CV 1000th cycles. b) HRTEM image of Act-HEO at CV 1000th cycles of the bulk and surface c-e), g) and h) FT-EXAFS for Zn, Cr, Mn, Fe, Co and Ni K-edge of Act-HEO at 1000th cycles. Fittings of experimental spectra obtained for HEO are shown in colored lines. i-k) XPS of O 2s, Co 2p$^{3/2}$ and Ni 2p$^{3/2}$ regions for the surface of Pri-HEO and Act-HEO at CV 1000th cycles.

The detailed surface cation compositions are shown in Figure 3a and Table S3. It is evident that surface Zn and Cr tend to leach out from the HEO, and the percentage of surface Co and Mn increases while that of the surface Fe and Ni remains the same. In addition, inductively concerted plasma mass spectrometry (ICP-MS) was used to explore the cation ratio in electrolyte. As shown in Figure S6, the concentration of Co and Mn cations in the electrolyte remains unchanged regardless of the electrochemical cycling. However, the mass of Cr, Ni and Fe observed in the electrolyte, which are leached from the catalyst, shows a linear increase during the process of CV cycling. The amount of leached Zn also increases as electrochemical cycling processes, but at a higher rate than the case of the other cations. The rate of Zn leaching even accelerates after 1500 cycles. Based on this information, it can be inferred that among all cations in HEO, Zn at the tetrahedral site shows the highest mobility to leach out from the structure. As a control experiment, the HEO electrode was soaked in KOH for 12 hours, The cation concentrations in the electrolyte remains low (Figure S6), indicating the presents of cation in the electrolyte was due to the leaching of surface cations during OER process. In addition, a TEM EDS-line scan was conducted to further investigate the elemental composition of the surface layer of high entropy (oxy)hydroxide after activation. For the pristine HEO catalyst, the stoichiometric proportion of octahedral site cation species on the surface is found to be similar to the as-synthesized bulk counterpart, as shown in Figure 3b. However, the surface profile of Act-HEO (after 1000 CV cycling) shows a significant depletion of Zn and an abundance of Co and Mn cations (Figure 3c).

To further analyze the increase in OER activity after the formation of surface MO_xH_y, the surface configurational entropy (S_{config}) was calculated. The contribution of the anion site is expected to have a minor influence on S_{config}, given that only one anion is present.[17, 22] The relationship between reconstructed MO_xH_y surface entropy and electrochemical performance at 1.6V vs. RHE is shown in Figure S7. The surface entropy is obtained from the XPS results (Figure 3a and Table S2). From the 200th to the 2000th CV cycle, the surface entropy ranges between ~ 1.73 R to ~ 1.76 R.

Therefore, combing the electrochemical and the surface analysis results, we can propose a full surface evolution process of HEO during OER. First, in the case of Pri-HEO, the surface lattice oxygen was involved during the OER process. In addition, some of the surface cations leached into the electrolyte, which results in the formation of a thin surface layer of metal (oxy)hydroxide (MO_xH_y) (Figure 3d) and enhances the metal-oxygen covalency. In addition, the participation of

surface lattice oxygen results in the formation of V_O, which further reduces the percentage of surface lattice oxygen. The enhanced metal-oxygen covalency and reduced surface lattice oxygen alters the OER pathway from non-concerted proton-electron transfer to concerted proton-electron transfer, resulting in a change in the RDS from step 1 to step 2. Second, the thickness of this newly formed layer stopped growing after around 200 cycles, which marks the point at which the OER pathway was fully converted. Third, due to the leaching of surface cations, the composition of this newly formed MO_xH_y layer undergoes continuous change. These surface composition changes influence the surface entropy, which in turn affects the OER activity of the catalyst. As Zn accounts for the largest proportion of the surface cations, volcano plots relating the surface entropy and Zn percentage in both experimental data and in the ideal case are observed (Figure 3e). In the ideal case where all other factors remain equal, the OER performance is expected to reach its highest level when the Zn percentage is equal to that of the other surface cations. Experimentally, there is a volcano-shaped relationship between the Zn percentage and surface entropy. However, the leaching of other surface cations results in a different situation compared to the ideal case. The experimental volcano peak is shifted forward compared to the ideal case, located at the point where ~ 70% of Zn remains on the surface, with the corresponding highest surface entropy of 1.762 R and a current density of 0.3 mA cm^{-2}_{ox}. In addition, the activity of HEO after 1500 times of CV cycling decreased while the surface percentage of Co and Ni increased. Although Co and Ni are more active than other metals for OER process,[2,3] the increased percentage of Co and Ni did not give a higher OER activity of HEO. However, the surface entropy of the newly formed HEH decreased. The observed relationship between surface entropy and oxidation activity indicates that surface entropy has a remarkable effect on oxidation activity, which has not been reported previously.

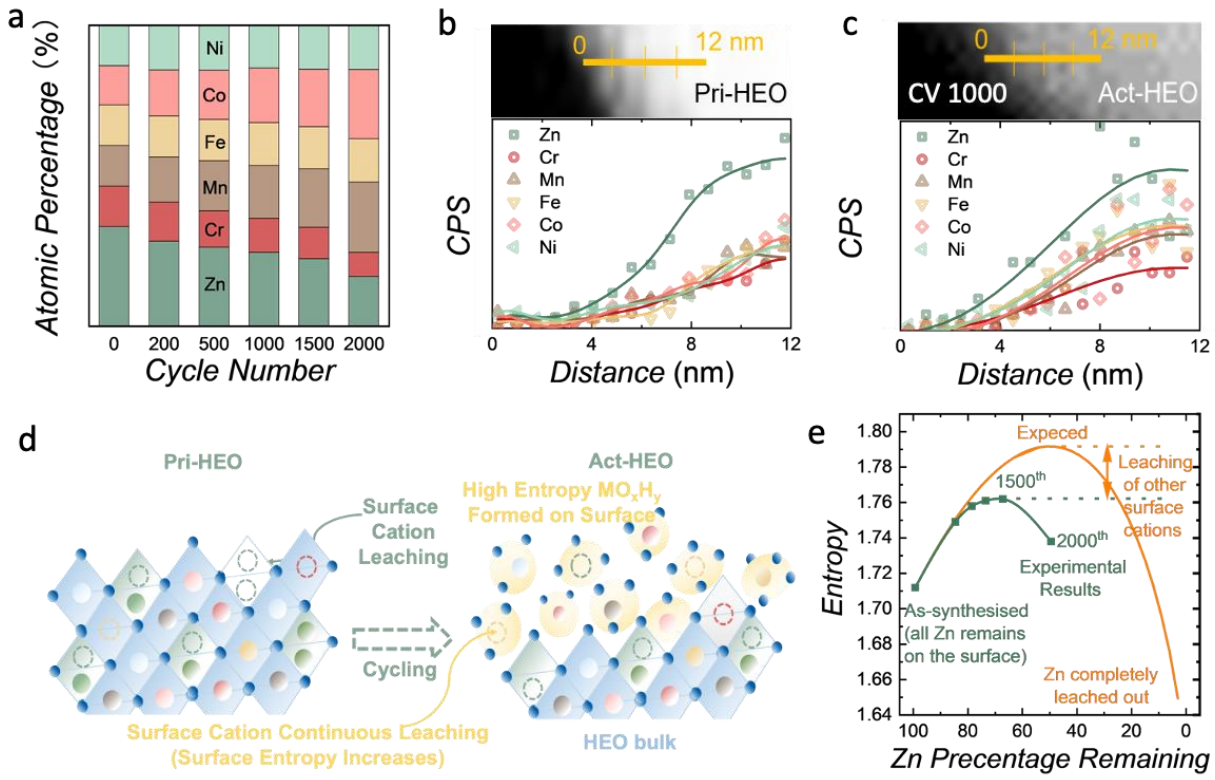

Figure 3: Evaluation of surface entropy and OER activity. a) X-ray photoelectron spectroscopy (XPS) surface cations (Zn, Cr, Mn, Fe, Co and Ni) atomic percentage of Pri-HEO and Act-HEO at 200th, 500th, 1000th, 1500th and 2000th cycles. b) - c) HRTEM-EDS image and line-scan of surface cation distribution for Pri-HEO and Act-HEO. d) Diagram of surface reconstruction process during OER. e) Relationship diagram between surface entropy and Zn percentage.

Comparison between high entropy and medium entropy compounds

The many different cations in the transition metal-based HEO makes it possible to exclude a specific element and investigate the resulting change in electrochemical behavior, thus allowing for the assignment of specific electrochemical characteristics to the absence of a particular element. Such an exclusion of one of the elements from a 6-cation system results in a significant decrease in the configurational entropy of the material from ~ 1.71 R to ~ 1.56 R. A series of these entropy-reduced transition metal-based-oxides (transition-metal-based medium entropy oxides, TM-MEOs) were synthesized using the same sol-gel method as TM-HEO. Figure 4a shows the X-ray

diffraction (XRD) pattern of the five 5-cation systems (TM-MEO) with no Cr, Mn, Fe, Co, or Ni, respectively (MEO-Cr, MEO-Mn, MEO-Fe, MEO-Co, and MEO-Ni). All the catalysts exhibit a cubic-spinel structure with the Fd3m space group. In addition, the EXAFS result for the Zn K-edge in Figure 4b shows that, for all MEO catalysts, the distances between Zn ions and their neighboring metal cations are around 3.0 Å, indicating that Zn ions accommodate the center of tetrahedrons for all TM-MEO samples (Figure 4b).[25, 26] However, as shown in Figure S2 and Table S1, the BET surface area values of the samples vary from 68 m^2 g^{-1} to 13 m^2 g^{-1}. As the same synthesis method was employed for each sample, the significant variation in the surface area is due to the difference in elemental composition. It is worth noting that MEO-Cr has the smallest BET area among all the synthesized HEO/MEO catalysts. It implies that the addition of Cr in the spinel structure can enlarge particle size.

To exclude the effect of surface area, the intrinsic OER activity results of the TM-HEO/MEO catalysts were normalized by the BET specific surface area.[43] In a long-term experiment with over 1000 CV cycling (Figure 4c-h and Figure S12), it is shown that the 6-cation sintered HEO system can exhibit a specific current density up to 250 μA cm^{-2} at 1.6 V vs. RHE for thousands of cycles. As for the results obtained from the MEOs, their comparatively lower current densities demonstrate that even the removal of a single element leads to significant changes in the electrochemical properties. However, the removal of different elements has subtly different effects on OER performance. Except for MEO-Ni, all other MEO catalysts show increasing performance for different durations. Removing Ni (MEO-Ni) leads to a monotonic decrease in performance as electrochemical cycling processes (Figure S5), which indicates that Ni is likely to be the active site for the OER catalysts. In contrast, the removal of Co, Mn, and Fe (MEO-Co, MEO-Mn, and MEO-Fe) does not impede the increase-decrease of OER performance. As for MEO-Cr, the activation period is shorter, which implies that the existence of Cr contributes to surface reconstruction. This effect was also mentioned in our previous work.[44] Other than that, the ICP result and electrochemical behavior of HEO also mean that Zn and Cr may have a combined effect, promoting surface reconstruction during the OER process.

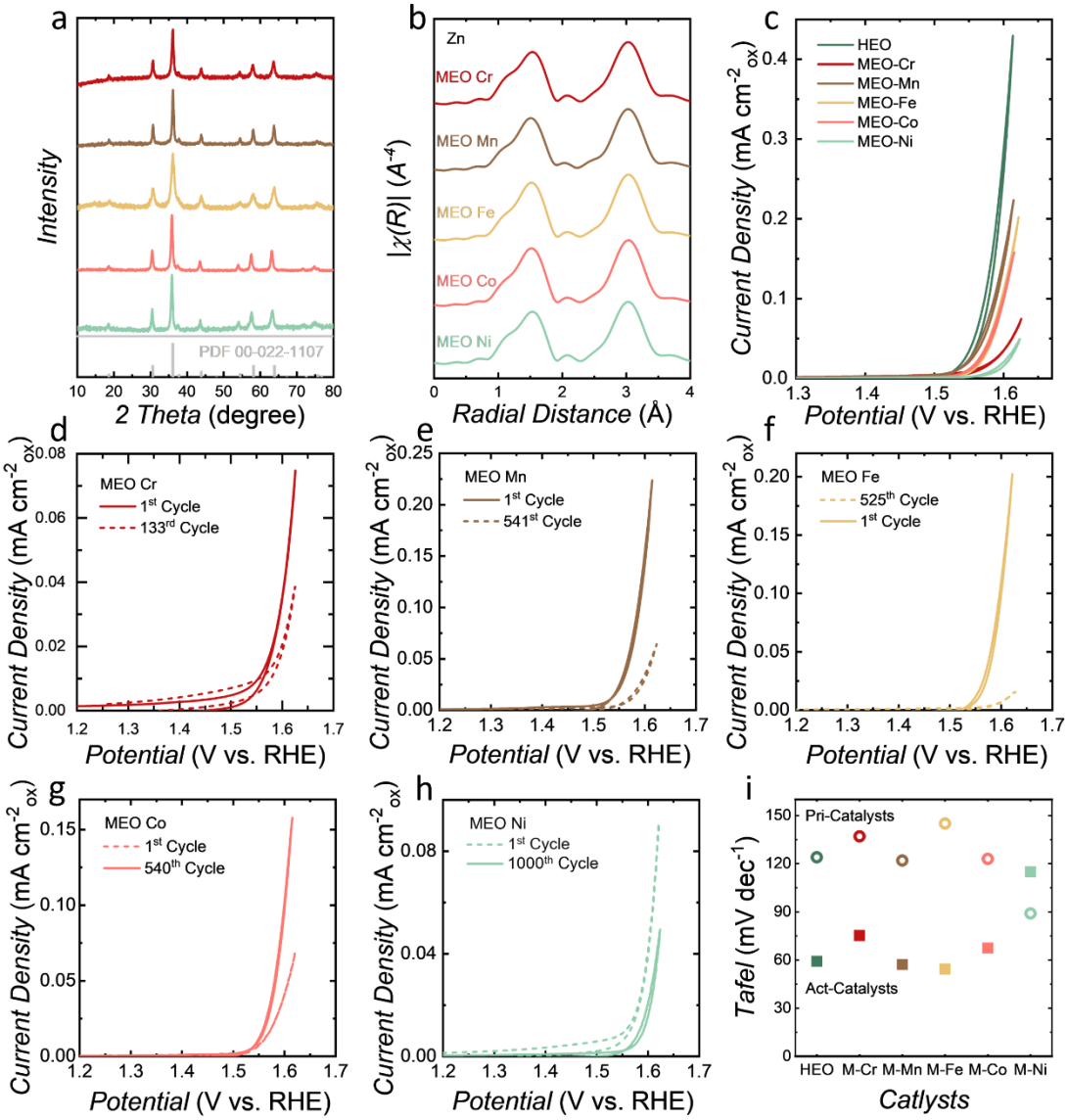

Figure 4: Comparison between HEO and MEOs. a) Powder XRD patterns of the as-synthesized TM-MEO catalysts. b) Fourier transform of the EXAFS (FT-EXAFS) for Zn K-edge of as-synthesized TM-MEOs. c) Comparison of current density (@ 1.6V vs. RHE) between HEO and MEOs. The current density was taken at 1.6 V vs. RHE at the highest performed cycle. d)-h) BET surface area normalized OER performance of TM-MEO catalysts (MEO-Cr, MEO-MN, MEO-Fe, MEO-Co, and MEO-Ni). i) Comparation of Tafel values between HEO and MEOs. The value was taken at the highest performed cycle.

For all the TM-HEO/MEO catalysts, the electrochemical results show similar increasing-decreasing behaviors and ICP-MS results show similar leaching phenomenon. Thus, we propose

that the MEO catalysts undergo the same surface evolution process as HEO. However, even though the initial capacity of MEOs does not differ much from the 6-cation system, the water oxidation activity shows a rapid drop after only 500 cycles (Figure 4c-h). Based on this, we also propose that the surface entropy changes more rapidly in the case of MEOs as compared to HEO. Furthermore, the ICP results show that more cations are leached into the electrolyte during the OER process after 1000 CV cycles than in the case of HEO (Figure S9), which implies that these cations are leached more rapidly in MEOs than in HEOs. Thus, the ICP results support the proposition of quicker entropy change during OER, which also suggests that HEO has a more stable structure than MEOs.

It should be noted that MEOs have a relatively less stable electrochemical performance compared to HEO. The MEOs, although initially displaying comparable OER activity as HEO, show varying degrees of degradation at around 500 cycles. In contrast, the 6-cation HEO displays a high activity that does not degrade with increasing electrochemical cycling. This difference in stability leads us to conclude that the HEO exhibits an entropy stabilization effect. Similar behavior has also been reported by other groups.[9] On the other hand, including or excluding one or two cations into the single-phase structure could open new possibilities for developing a modular method to tailor electrodes suited to different needs. The HEO concept, with its countless possible cation combinations, clearly offers unique opportunities to tailor electrochemical properties in a flexible way.

Conclusion

A spinel type high entropy oxide $Zn(CrMnFeCoNi)_2O_4$ has been identified as a highly active OER catalyst. By induced leaching of surface Zn from tetrahedral sites, It has been found that electrochemical cycling of this HEO results in surface reconstruction with surface Zn leaching and a completely new phase of high entropy metal (oxy)hydroxide is observed on the surface. An increase in surface entropy over the pristine spinel HEO has been observed. The newly formed surface exhibits improved OER catalytic performance. Additionally, varying the composition of the oxides allows tailoring the OER performance. The entropy stabilization effect has been found to have a positive effect on OER performance. In essence, incorporating different elements into HEOs offers a modular approach for the systematic design of the anode catalysts in water splitting.

These results reveal the vast potential of engineering high entropy oxides for advanced electrocatalytic applications.

Supporting Information

The Supporting Information is available free of charge at https://pubs.acs.org/doi/xxx. More materials characterizations such as TEM, BET, SEM, EDS mapping, XPS spectra of Pri-HEO and Act-HEO CV-cycled with different cycles, ICP results of electrolytes after cycling, etc.

Acknowledgements

The authors thank the financial support from Agency for Science, Technology and Research (A*STAR) MTC Individual Research Grants (IRG) M22K2c0078. Y. Sun thanks the financial support from the National Natural Science Foundation of China (No. 52373233), the SIAT International Joint Lab Project (No. E3G113), and Shenzhen Science and Technology Program (KQTD20221101093647058).

Conflict of Interests

The authors declare no competing interests.

Reference

(1) Turner, J. A. Sustainable Hydrogen Production. *Science* **2004**, *305* (5686), 972-974. DOI: doi:10.1126/science.1103197.

(2) Wu, T.; Sun, Y.; Ren, X.; Wang, J.; Song, J.; Pan, Y.; Mu, Y.; Zhang, J.; Cheng, Q.; Xian, G.; et al. Reconstruction of Thiospinel to Active Sites and Spin Channels for Water Oxidation. *Advanced Materials* **2023**, *35* (2), 2207041. DOI: https://doi.org/10.1002/adma.202207041.

(3) Sun, Y.; Wang, J.; Xi, S.; Shen, J.; Luo, S.; Ge, J.; Sun, S.; Chen, Y.; Hanna, J. V.; Li, S.; et al. Navigating surface reconstruction of spinel oxides for electrochemical water oxidation. *Nature Communications* **2023**, *14* (1), 2467. DOI: 10.1038/s41467-023-38017-3.

(4) Chen, Y.; Seo, J. K.; Sun, Y.; Wynn, T. A.; Olguin, M.; Zhang, M.; Wang, J.; Xi, S.; Du, Y.; Yuan, K.; et al. Enhanced oxygen evolution over dual corner-shared cobalt tetrahedra. *Nature Communications* **2022**, *13* (1), 5510. DOI: 10.1038/s41467-022-33000-w.

(5) Luo, S.; Elouarzaki, K.; Xu, Z. J. Electrochemistry in Magnetic Fields. *Angewandte Chemie International Edition* **2022**, *61* (27), e202203564. DOI: https://doi.org/10.1002/anie.202203564.

(6) An, L.; Wei, C.; Lu, M.; Liu, H.; Chen, Y.; Scherer, G. G.; Fisher, A. C.; Xi, P.; Xu, Z. J.; Yan, C.-H. Recent Development of Oxygen Evolution Electrocatalysts in Acidic Environment. *Advanced Materials* **2021**, *33* (20), 2006328. DOI: https://doi.org/10.1002/adma.202006328.

(7) Li, J.; Zheng, G. One-Dimensional Earth-Abundant Nanomaterials for Water-Splitting Electrocatalysts. *Advanced Science* **2017**, *4* (3), 1600380. DOI: https://doi.org/10.1002/advs.201600380.

(8) Chen, Y.; Li, H.; Wang, J.; Du, Y.; Xi, S.; Sun, Y.; Sherburne, M.; Ager III, J. W.; Fisher, A. C.; Xu, Z. J. Exceptionally active iridium evolved from a pseudo-cubic perovskite for oxygen evolution in acid. *Nature communications* **2019**, *10* (1), 572.

(9) Yin, J.; Li, Y.; Lv, F.; Lu, M.; Sun, K.; Wang, W.; Wang, L.; Cheng, F.; Li, Y.; Xi, P. Oxygen vacancies dominated NiS2/CoS2 interface porous nanowires for portable Zn–air batteries driven water splitting devices. *Advanced Materials* **2017**, *29* (47), 1704681.

(10) Wei, Y.; Zheng, Y.; Hu, Y.; Huang, B.; Sun, M.; Da, P.; Xi, P.; Yan, C.-H. Controlling the cation exsolution of perovskite to customize heterostructure active site for oxygen evolution reaction. *ACS Applied Materials & Interfaces* **2022**, *14* (22), 25638-25647.

(11) Suen, N.-T.; Hung, S.-F.; Quan, Q.; Zhang, N.; Xu, Y.-J.; Chen, H. M. Electrocatalysis for the oxygen evolution reaction: recent development and future perspectives. *Chemical Society Reviews* **2017**, *46* (2), 337-365.

(12) Liu, X.; Meng, J.; Zhu, J.; Huang, M.; Wen, B.; Guo, R.; Mai, L. Comprehensive understandings into complete reconstruction of precatalysts: synthesis, applications, and characterizations. *Advanced Materials* **2021**, *33* (32), 2007344.

(13) Fabbri, E.; Nachtegaal, M.; Binninger, T.; Cheng, X.; Kim, B.-J.; Durst, J.; Bozza, F.; Graule, T.; Schäublin, R.; Wiles, L. Dynamic surface self-reconstruction is the key of highly active perovskite nano-electrocatalysts for water splitting. *Nature materials* **2017**, *16* (9), 925-931.

(14) Burke, M. S.; Kast, M. G.; Trotochaud, L.; Smith, A. M.; Boettcher, S. W. Cobalt–iron (oxy) hydroxide oxygen evolution electrocatalysts: the role of structure and composition on activity, stability, and mechanism. *Journal of the American Chemical Society* **2015**, *137* (10), 3638-3648.

(15) Duan, Y.; Sun, S.; Sun, Y.; Xi, S.; Chi, X.; Zhang, Q.; Ren, X.; Wang, J.; Ong, S. J. H.; Du, Y.; et al. Mastering Surface Reconstruction of Metastable Spinel Oxides for Better Water Oxidation. *Advanced Materials* **2019**, *31* (12), 1807898. DOI: https://doi.org/10.1002/adma.201807898.

(16) Sun, Y.; Dai, S. High-entropy materials for catalysis: A new frontier. *Science Advances* **2021**, *7* (20), eabg1600. DOI: doi:10.1126/sciadv.abg1600.

(17) Sarkar, A.; Velasco, L.; Wang, D.; Wang, Q.; Talasila, G.; de Biasi, L.; Kübel, C.; Brezesinski, T.; Bhattacharya, S. S.; Hahn, H.; Breitung, B. High entropy oxides for reversible energy storage. *Nature Communications* **2018**, *9* (1), 3400. DOI: 10.1038/s41467-018-05774-5.

(18) Sarkar, A.; Wang, Q.; Schiele, A.; Chellali, M. R.; Bhattacharya, S. S.; Wang, D.; Brezesinski, T.; Hahn, H.; Velasco, L.; Breitung, B. High-Entropy Oxides: Fundamental Aspects and

Electrochemical Properties. *Advanced Materials* **2019**, *31* (26), 1806236. DOI: https://doi.org/10.1002/adma.201806236.

(19) Jia, Z.; Nomoto, K.; Wang, Q.; Kong, C.; Sun, L.; Zhang, L.-C.; Liang, S.-X.; Lu, J.; Kruzic, J. J. A Self-Supported High-Entropy Metallic Glass with a Nanosponge Architecture for Efficient Hydrogen Evolution under Alkaline and Acidic Conditions. *Advanced Functional Materials* **2021**, *31* (38), 2101586. DOI: https://doi.org/10.1002/adfm.202101586.

(20) Anand, G.; Wynn, A. P.; Handley, C. M.; Freeman, C. L. Phase stability and distortion in high-entropy oxides. *Acta Materialia* **2018**, *146*, 119-125. DOI: https://doi.org/10.1016/j.actamat.2017.12.037.

(21) Sarkar, A.; Breitung, B.; Hahn, H. High entropy oxides: The role of entropy, enthalpy and synergy. *Scripta Materialia* **2020**, *187*, 43-48. DOI: https://doi.org/10.1016/j.scriptamat.2020.05.019.

(22) Rost, C. M.; Sachet, E.; Borman, T.; Moballegh, A.; Dickey, E. C.; Hou, D.; Jones, J. L.; Curtarolo, S.; Maria, J.-P. Entropy-stabilized oxides. *Nature Communications* **2015**, *6* (1), 8485. DOI: 10.1038/ncomms9485.

(23) Praveen, S.; Kim, H. S. High‐entropy alloys: potential candidates for high‐temperature applications–an overview. *Advanced Engineering Materials* **2018**, *20* (1), 1700645.

(24) Sathiyamoorthi, P.; Kim, H. S. High-entropy alloys with heterogeneous microstructure: processing and mechanical properties. *Progress in Materials Science* **2022**, *123*, 100709.

(25) Wang, M.; Árnadóttir, L.; Xu, Z. J.; Feng, Z. In Situ X-ray Absorption Spectroscopy Studies of Nanoscale Electrocatalysts. *Nano-Micro Letters* **2019**, *11* (1), 47. DOI: 10.1007/s40820-019-0277-x.

(26) Robouch, B. V.; Kisiel, A. EXAFS data resolved into individual site occupation preferences in quaternary compounds with tetrahedral coordinated structure. *Journal of Alloys and Compounds* **1999**, *286* (1), 80-88. DOI: https://doi.org/10.1016/S0925-8388(98)00984-0.

(27) Sommer, S.; Bøjesen, E. D.; Lock, N.; Kasai, H.; Skibsted, J.; Nishibori, E.; Iversen, B. B. Probing the validity of the spinel inversion model: a combined SPXRD, PDF, EXAFS and NMR study of ZnAl2O4. *Dalton Transactions* **2020**, *49* (38), 13449-13461, 10.1039/D0DT02795B. DOI: 10.1039/D0DT02795B.

(28) Henderson, C. M. B.; Charnock, J. M.; Plant, D. A. Cation occupancies in Mg, Co, Ni, Zn, Al ferrite spinels: a multi-element EXAFS study. *Journal of Physics: Condensed Matter* **2007**, *19* (7), 076214. DOI: 10.1088/0953-8984/19/7/076214.

(29) Sun, S.; Li, H.; Xu, Z. J. Impact of Surface Area in Evaluation of Catalyst Activity. *Joule* **2018**, *2* (6), 1024-1027. DOI: https://doi.org/10.1016/j.joule.2018.05.003.

(30) Wei, C.; Xu, Z. J. The Comprehensive Understanding of as an Evaluation Parameter for Electrochemical Water Splitting. *Small Methods* **2018**, *2* (11), 1800168. DOI: https://doi.org/10.1002/smtd.201800168.

(31) Grimaud, A.; Diaz-Morales, O.; Han, B.; Hong, W. T.; Lee, Y. L.; Giordano, L.; Stoerzinger, K. A.; Koper, M. T. M.; Shao-Horn, Y. Activating lattice oxygen redox reactions in metal oxides

to catalyse oxygen evolution. *Nature chemistry* **2017**, *9* (5), 457-465. DOI: 10.1038/nchem.2695 From NLM.

(32) Sun, S.; Sun, Y.; Zhou, Y.; Shen, J.; Mandler, D.; Neumann, R.; Xu, Z. J. Switch of the rate-determining step of water oxidation by spin-selected electron transfer in spinel oxides. *Chemistry of Materials* **2019**, *31* (19), 8106-8111.

(33) Maurya, R.; Das, R.; Tripathi, A. K.; Neergat, M. Relationship between the electron-transfer coefficients of the oxygen reduction reaction estimated from the Gibbs free energy of activation and the Butler–Volmer equation. *Physical Chemistry Chemical Physics* **2023**, *25* (1), 700-707.

(34) Zhou, Y.; Sun, S.; Song, J.; Xi, S.; Chen, B.; Du, Y.; Fisher, A. C.; Cheng, F.; Wang, X.; Zhang, H.; Xu, Z. J. Enlarged Co□O Covalency in Octahedral Sites Leading to Highly Efficient Spinel Oxides for Oxygen Evolution Reaction. *Advanced Materials* **2018**, *30* (32), 1802912. DOI: https://doi.org/10.1002/adma.201802912.

(35) Rong, X.; Parolin, J.; Kolpak, A. A fundamental relationship between reaction mechanism and stability in metal oxide catalysts for oxygen evolution. ACS Catal. 6, 1153–1158. 2016.

(36) Grimaud, A.; Diaz-Morales, O.; Han, B.; Hong, W. T.; Lee, Y.-L.; Giordano, L.; Stoerzinger, K. A.; Koper, M. T.; Shao-Horn, Y. Activating lattice oxygen redox reactions in metal oxides to catalyse oxygen evolution. *Nature chemistry* **2017**, *9* (5), 457-465.

(37) Yang, C.; Grimaud, A. Factors controlling the redox activity of oxygen in perovskites: from theory to application for catalytic reactions. *Catalysts* **2017**, *7* (5), 149.

(38) Chastain, J.; King Jr, R. C. Handbook of X-ray photoelectron spectroscopy. *Perkin-Elmer, USA* **1992**, 261.

(39) Yang, J.; Liu, H.; Martens, W. N.; Frost, R. L. Synthesis and Characterization of Cobalt Hydroxide, Cobalt Oxyhydroxide, and Cobalt Oxide Nanodiscs. *The Journal of Physical Chemistry C* **2010**, *114* (1), 111-119. DOI: 10.1021/jp908548f.

(40) Liardet, L.; Hu, X. Amorphous Cobalt Vanadium Oxide as a Highly Active Electrocatalyst for Oxygen Evolution. *ACS Catalysis* **2018**, *8* (1), 644-650. DOI: 10.1021/acscatal.7b03198.

(41) Stoerzinger, K. A.; Hong, W. T.; Crumlin, E. J.; Bluhm, H.; Biegalski, M. D.; Shao-Horn, Y. Water Reactivity on the LaCoO3 (001) Surface: An Ambient Pressure X-ray Photoelectron Spectroscopy Study. *The Journal of Physical Chemistry C* **2014**, *118* (34), 19733-19741. DOI: 10.1021/jp502970r.

(42) Shen, Z.; Zhuang, Y.; Li, W.; Huang, X.; Oropeza, F. E.; Hensen, E. J. M.; Hofmann, J. P.; Cui, M.; Tadich, A.; Qi, D.; et al. Increased activity in the oxygen evolution reaction by Fe4+-induced hole states in perovskite La1−xSrxFeO3. *Journal of Materials Chemistry A* **2020**, *8* (8), 4407-4415, 10.1039/C9TA13313E. DOI: 10.1039/C9TA13313E.

(43) Roy, C.; Sebok, B.; Scott, S. B.; Fiordaliso, E. M.; Sørensen, J. E.; Bodin, A.; Trimarco, D. B.; Damsgaard, C. D.; Vesborg, P. C. K.; Hansen, O.; et al. Impact of nanoparticle size and lattice oxygen on water oxidation on NiFeOxHy. *Nature Catalysis* **2018**, *1* (11), 820-829. DOI: 10.1038/s41929-018-0162-x.

(44) Duan, Y.; Lee, J. Y.; Xi, S.; Sun, Y.; Ge, J.; Ong, S. J. H.; Chen, Y.; Dou, S.; Meng, F.; Diao, C.; et al. Anodic Oxidation Enabled Cation Leaching for Promoting Surface Reconstruction in

Water Oxidation. *Angewandte Chemie International Edition* **2021**, *60* (13), 7418-7425. DOI: https://doi.org/10.1002/anie.202015060.

TOC